Barotropic instability of a zonal jet on the sphere: from non-divergence through quasi-geostrophy to shallow water

Nathan Paldor, Ofer Shamir & Chaim. I. Garfinkel

Published online: 24 Feb 2020.

Submit your article to this journal ↗

Article views: 249

View related articles ↗

View Crossmark data ↗

Barotropic instability of a zonal jet on the sphere: from non-divergence through quasi-geostrophy to shallow water

Nathan Paldor [ID], Ofer Shamir and Chaim. I. Garfinkel

Fredy and Nadine Herrmann Institute of Earth Sciences, The Hebrew University of Jerusalem, Jerusalem, Israel

ABSTRACT

Two common approximations to the full Shallow Water Equations (SWEs) are non-divergence and quasi-geostrophy, and the degree to which these approximations lead to biases in numerical solutions are explored using the test bed of barotropic instability. Specifically, we examine the linear stability of strong polar and equatorial jets and compare the growth rates obtained from the SWEs along with those obtained from the Non-Divergent barotropic vorticity (ND) equation and the Quasi-Geostrophic (QG) equation. The main result of this paper is that the depth over which a layer is barotropically unstable is a crucial parameter in controlling the growth rate of small amplitude perturbations and this dependence is completely lost in the ND equation and is overly weak in the QG system. Only for depths of 30 km or more are the growth rates predicted by the ND and QG systems a good approximation to those of the SWEs, and such a convergence for deep layers can be explained using theoretical considerations. However, for smaller depths, the growth rates predicted by the SWEs become smaller than those of the ND and QG systems and for depths of between 5 and 10 km they can be smaller by more than 50%. For polar jets, and for depths below 2 km the mean height in geostrophic balance with the strong zonal jet becomes negative and hence the barotropic instability problem is ill-defined. While in the SWEs an equatorial jet becomes stable for layer depths smaller than 3–4 km, in the QG and ND approximations it is unstable for layer depths down to 1 km. These result may have implications for the importance of barotropic instability in Earth's upper stratosphere and perhaps also other planets such as Venus.

1. Introduction

The theory of barotropic instability has its roots over half a century ago in the pioneering works of Kuo (1949, 1973) in which he studied the exponential temporal growth of small wavelike perturbations added to a zonal westerly jet in a zonal channel on the β-plane. Kuo based his theory on the Non-Divergent (ND) vorticity equation, which was also the basis of many barotropic instability studies throughout the second half of the twentieth century. These studies were aimed at differentiating between stable and unstable mean flows in order to identify states that are expected to change rapidly due to the exponential

CONTACT Nathan Paldor ✉ nathan.paldor@huji.ac.il

temporal growth of small amplitude perturbations. Later studies examined settings that are more complex than the ND vorticity equation, such as the Quasi-Geostrophic (QG) equation (e.g. Hartmann 1983) and the Shallow Water Equations (SWEs) (e.g. Paldor and Dvorkin 2006).

The ND and QG approximations, that together constitute the primary approximate systems used in the development of Geophysical Fluid Dynamics (GFD) for 70 years, can be derived as asymptotic limits of the SWEs at small Rossby number when the length and velocity scales are determined either by initial conditions or inhomogeneous (forcing) terms (e.g. Reznik *et al.* 2001, Rostami and Zeitlin 2019). Such auxiliary scales do not exist in a linear boundary (eigenvalue) problem on a sphere where the only boundary conditions are regularity of the solutions at the (singular) poles. Alternate derivations of the approximate QG and ND systems require either setting to zero a derived quantity (e.g. divergence, in the case of the ND system) or by limiting the values of several parameters and (yet unknown) variables (i.e. deviation of velocity from the geostrophic velocity, β-term, frequency, the length scale of the flow, in the case of the QG system). In this, latter, way of deriving the approximate ND and QG systems it is important to establish the regimes where their solutions can be expected to provide acceptable approximations to solutions of the SWEs.

In this work we compare the growth rates of barotropic instability on a zonal jet in the ND, QG, and SWEs systems when each system is linearised about the same mean wind profile. The use of the same basic state in the three systems clarifies how the assumptions made in formulating the perturbation equation affect the subsequent growth rates in each system. As discussed above, the QG and ND equations can be derived from the SWEs by implementing a series of approximations. More restrictive approximations are implemented in the ND system (including non-divergence of the two-dimensional velocity field) compared to the QG system. The more general SWEs with no approximations can be related to the underlying primitive equations that govern atmospheric motion (Vallis 2006, Zeitlin 2018), and for the case of a sufficiently simple temperature profile barotropic instability in the atmosphere is identical to that in the SWEs (Chapman and Lindzen 1970, Andrews *et al.* 1987).

We solve for unstable modes of both strong polar and equatorial jets on the sphere for a range of layer depths typical to Earth, and find that, for depths of about 10 km or less, jets reminiscent of the one observed in the Southern Hemisphere polar stratosphere and in the Quasi Biennial Oscillation are more stable when using the SWEs or QG equation than in the non-divergent equation. The degree to which the growth rates are smaller depends on the depth for a given mean state wind profile, and for depths of less than 5 km e-folding times exceed 10 days for the SWEs. Only for layer depths exceeding 30 km are the growth rates derived from the SWEs similar to those of the non-divergent equation. This difference in e-folding time scale is due to rather subtle differences in the eigenfunctions of the normal modes. The implication of this result is that the depth over which a jet is barotropically unstable is a crucial parameter in controlling its growth rate. We focus here on relatively simple barotropic wind profiles and focus exclusively on barotropic instability. However, we acknowledge that a thin layer of potential vorticity reversal may grow even faster if baroclinic instability is also present, as in Earth's upper stratosphere or lower mesosphere, but a detailed consideration of this effect is beyond the scope of the present work which focuses on barotropic instability only.

In section 2 we introduce the governing equations of the three systems and derive the corresponding equations for the basic state and linear response with respect to a zonal mean flow. Section 3 provides a more detailed discussion with regard to the relations between the three system and the conditions under which they can be expected to converge. In section 4 we demonstrate the differences between the three systems in the particular case of barotropic instability of a zonal jet on the sphere. The results are summarised and discussed in section 5.

2. Governing equations and methods of solution

In order to study the effects of divergence on the growth rates of barotropic instability we compare the growth rates obtained from the rotating spherical Shallow Water Equations (SWEs) with those from the non-divergent barotropic vorticity equation, and with those from the Quasi-Geostrophic (QG) equation. In this section we present the equations in the three systems and the methods of solution used in calculating the growth rates.

2.1. Shallow water system

The SWEs on the rotating spherical Earth are given by (see e.g. Gill 1982)

$$\frac{\partial u}{\partial t} + \frac{u}{a\cos\phi}\frac{\partial u}{\partial \lambda} + \frac{v}{a}\frac{\partial u}{\partial \phi} - \left[2\Omega + \frac{u}{a\cos\phi}\right]v\sin\phi = -\frac{g}{a\cos\phi}\frac{\partial h}{\partial \lambda}, \quad (1a)$$

$$\frac{\partial v}{\partial t} + \frac{u}{a\cos\phi}\frac{\partial v}{\partial \lambda} + \frac{v}{a}\frac{\partial v}{\partial \phi} + \left[2\Omega + \frac{u}{a\cos\phi}\right]u\sin\phi = -\frac{g}{a}\frac{\partial h}{\partial \phi}, \quad (1b)$$

$$\frac{\partial h}{\partial t} + \frac{u}{a\cos\phi}\frac{\partial h}{\partial \lambda} + \frac{v}{a}\frac{\partial h}{\partial \phi} + \frac{h}{a\cos\phi}\left[\frac{\partial u}{\partial \lambda} + \frac{\partial(v\cos\phi)}{\partial \phi}\right] = 0, \quad (1c)$$

where λ, ϕ and t are the longitude, latitude and time, respectively; u, v and h are the zonal velocity, meridional velocity and layer's thickness (measured here from a flat bottom), respectively; and a, g and Ω denote Earth's mean radius, gravitational acceleration and angular frequency, respectively. As discussed in detail in Chapman and Lindzen (1970) and Zeitlin (2018), the SWEs can be derived from the full primitive equations if the vertical structure of the background zonal wind and temperature is separable from the horizontal structure, or if a vertical average is performed between two atmospheric layers.

Since we are interested in the linear stability of small perturbations with respect to a zonal mean flow, in what follows we assume the following decomposition for u, v and h:

$$u = \bar{u}(\phi) + u'(\lambda, \phi, t), \quad (2a)$$

$$v = v'(\lambda, \phi, t), \quad (2b)$$

$$h = \underbrace{H + \bar{\eta}(\phi)}_{\bar{h}} + \eta'(\lambda, \phi, t), \quad (2c)$$

where $|u'|$, $|v'| \ll |\bar{u}|$ and $|\eta'| \ll |\bar{h}|$, and where the constant H is the layer's thickness in a motionless basic-state, i.e. when $\bar{u} = 0$. The zero- and first-order terms (i.e. terms containing zero and first powers of u', v' and η') describe the (steady) basic-state and the linear response of the perturbations, respectively, and are discussed below separately.

2.1.1. Basic-state

Substituting (2) into (1) and retaining only zero-order terms it follows that $\bar{u}$ and $\bar{\eta}$ must satisfy a (spherical) geostrophic balance (see, e.g. Andrews *et al.* 1987)

$$\left[2\Omega + \frac{\bar{u}}{a\cos\phi}\right]\bar{u}\sin\phi = -\frac{g}{a}\frac{\mathrm{d}\bar{\eta}}{\mathrm{d}\phi}. \tag{3}$$

In this work we assume a given (specified) zonal wind profile, $\bar{u}(\phi)$, in which case the corresponding mean height profile is given by

$$\bar{\eta}(\phi) = \bar{\eta}\left(-\tfrac{1}{2}\pi\right) - \frac{a}{g}\int_{-\pi/2}^{\phi}\left[2\Omega + \frac{\bar{u}}{a\cos\phi'}\right]\bar{u}\sin\phi'\,\mathrm{d}\phi'. \tag{4}$$

In addition to the zonal wind, a complete specification of the basic-state requires also the determination of the value of the mean height at a certain reference latitude, chosen here to be the south pole for convenience. In order to specify $\bar{\eta}(-\pi/2)$ in a meaningful way we further assume conservation of mass with respect to changes in the zonal wind. Specifically, we assume that the layer's total mass (or volume) equals its mass (or volume) in a motionless basic state, i.e. when $\bar{u} = 0$. Such a choice leads to the desired property that the layer's thickness in a motionless basic state, H, is approximately equal to the mean thickness after $\bar{u}$ is introduced, i.e. that the latitudinal average of $\bar{\eta}$ is approximately zero (see Appendix). This condition together with the geostrophic wind balance yields the following expression for the mean height field at the south pole (see Appendix)

$$\bar{\eta}\left(-\tfrac{1}{2}\pi\right) \approx \frac{a}{2g}\int_{-\pi/2}^{\pi/2}\mathrm{d}\phi\,\cos\phi\int_{-\pi/2}^{\phi}\left[2\Omega + \frac{\bar{u}}{a\cos\phi'}\right]\bar{u}\sin\phi'\,\mathrm{d}\phi'. \tag{5}$$

2.1.2. Linear perturbations

The first-order equations of system (1) are

$$\frac{\partial u'}{\partial t} + \frac{\bar{u}}{a\cos\phi}\frac{\partial u'}{\partial\lambda} + \frac{v'}{a}\frac{\mathrm{d}\bar{u}}{\mathrm{d}\phi} - \left[2\Omega + \frac{\bar{u}}{a\cos\phi}\right]v'\sin\phi = -\frac{g}{a\cos\phi}\frac{\partial\eta'}{\partial\lambda}, \tag{6a}$$

$$\frac{\partial v'}{\partial t} + \frac{\bar{u}}{a\cos\phi}\frac{\partial v'}{\partial\lambda} + \left[2\Omega + \frac{2\bar{u}}{a\cos\phi}\right]u'\sin\phi = -\frac{g}{a}\frac{\partial\eta'}{\partial\phi}, \tag{6b}$$

$$\frac{\partial\eta'}{\partial t} + \frac{\bar{u}}{a\cos\phi}\frac{\partial\eta'}{\partial\lambda} + \frac{v'}{a}\frac{\mathrm{d}\bar{\eta}}{\mathrm{d}\phi} + \frac{H+\bar{\eta}}{a\cos\phi}\left[\frac{\partial u'}{\partial\lambda} + \frac{\partial(v'\cos\phi)}{\partial\phi}\right] = 0. \tag{6c}$$

The substitution of zonally propagating wave solutions of the form

$$\{u', v', \eta'\} = \{\hat{u}(\phi), -\mathrm{i}\hat{v}(\phi), \hat{\eta}(\phi)\}\exp[\mathrm{i}(k\lambda - \omega t)], \tag{7}$$

where k and ω are the zonal wavenumber and frequency of the wave, respectively, yields the following eigenvalue problem for the latitude-dependent amplitudes $\{\hat{u}(\phi), \hat{v}(\phi), \hat{\eta}(\phi)\}$

in which ω is the eigenvalue

$$\omega\hat{u} = \frac{\bar{u}k}{a\cos\phi}\hat{u} + \left[2\Omega + \frac{\bar{u}}{a\cos\phi} - \frac{1}{a\sin\phi}\frac{d\bar{u}}{d\phi}\right]\hat{v}\sin\phi + \frac{gk}{a\cos\phi}\hat{\eta}, \tag{8a}$$

$$\omega\hat{v} = \left[2\Omega + \frac{2\bar{u}}{a\cos\phi}\right]\hat{u}\sin\phi + \frac{\bar{u}k}{a\cos\phi}\hat{v} + \frac{g}{a}\frac{d\hat{\eta}}{d\phi}, \tag{8b}$$

$$\omega\hat{\eta} = \frac{(H+\bar{\eta})k}{a\cos\phi}\hat{u} - \frac{H+\bar{\eta}}{a\cos\phi}\frac{d(\hat{v}\cos\phi)}{d\phi} - \frac{1}{a}\frac{d\bar{\eta}}{d\phi}\hat{v} + \frac{\bar{u}k}{a\cos\phi}\hat{\eta}. \tag{8c}$$

In section 4 we solve this system using both a Chebyshev collocation method and a shooting method in order to substantiate the results. For the shooting method it is convenient to re-write system (8) as a second-order system in $\hat{v}$ and $\hat{\eta}$ by using the first row in (8) to eliminate $\hat{u}$ form the second and third rows. The resulting second-order system is

$$(\omega - \bar{\omega})\cos\phi\frac{d\hat{V}}{d\phi} = \left[k(f+\bar{\zeta}) - \frac{(\omega-\bar{\omega})\cos\phi}{H+\bar{\eta}}\frac{d\bar{\eta}}{d\phi}\right]\hat{V} + \left[gk^2 - \frac{a(\omega-\bar{\omega})^2\cos^2\phi}{H+\bar{\eta}}\right]\hat{\eta}, \tag{9a}$$

$$(\omega - \bar{\omega})\cos\phi\frac{d\hat{\eta}}{d\phi} = \left[\frac{a(\omega-\bar{\omega})^2}{g} - \left(1+\frac{\bar{\omega}}{\Omega k}\right)\frac{af(f+\bar{\zeta})}{g}\right]\hat{V} - \left[\left(1+\frac{\bar{\omega}}{\Omega k}\right)kf\right]\hat{\eta}, \tag{9b}$$

where $\hat{V} = \hat{v}\cos\phi$, $\bar{\omega} = k\bar{u}/(a\cos\phi)$, $f = 2\Omega\sin\phi$ is the Coriolis parameter, and where

$$\bar{\zeta} = -\frac{1}{a\cos\phi}\frac{d(\bar{u}\cos\phi)}{d\phi} \tag{10}$$

is the relative vorticity of the mean zonal flow.

2.2. The non-divergent system

The non-divergent (ND) model reduces the order of the shallow water model from third-order in time to first-order in time by replacing the horizontal momentum equations with the vorticity-divergence ones and setting the divergence equal to zero. The resulting system consists of a single equation for the vorticity, namely the non-divergent barotropic vorticity equation, and two constraints: A boundary value problem, referred to as the 'balance equation', which relates the vorticity, horizontal velocity and free-surface height, and a constant (with respect to time) free-surface height. The resulting system after setting the divergence equal to zero is

$$\frac{\partial}{\partial t}\zeta + \frac{u}{a\cos\phi}\frac{\partial}{\partial\lambda}\zeta + \frac{v}{a}\frac{\partial}{\partial\phi}(\zeta + f) = 0, \tag{11a}$$

$$\boldsymbol{k}\cdot\nabla \times \left[(\zeta + f)\boldsymbol{u}\right] - \nabla^2\left[\tfrac{1}{2}\boldsymbol{u}\cdot\boldsymbol{u} + gh\right] = 0, \tag{11b}$$

$$h = h(\lambda, \phi), \tag{11c}$$

where $\boldsymbol{u} = (u, v)$ is the horizontal velocity vector, $\boldsymbol{k}$ is the unit vector in the vertical direction and

$$\zeta = \frac{1}{a\cos\phi}\left[\frac{\partial v}{\partial\lambda} - \frac{\partial(u\cos\phi)}{\partial\phi}\right] \tag{12}$$

is the relative vorticity. Note that the ND model in (11) is obtained from the SWEs model by taking the curl and divergence of the momentum equations and neglecting η' and $\bar{\eta}$ compared to H, which implies that the two models can be expected to converge in the asymptotic limit $1/H \to 0$ (see also Cho and Polvani 1996).

2.2.1. Basic-state

Assuming the same decomposition (2) as in the previous section it follows that $h = \bar{h}(\phi) = H + \bar{\eta}(\phi) + \eta'(\lambda)$, where $\bar{\eta}(\phi)$ is related to the mean zonal wind through the zero-order terms in the second row of (11). Upon assuming that $d\bar{\eta}/d\phi$ is regular at the poles, it follows that $\bar{\eta}(\phi)$ is related to $\bar{u}(\phi)$ through the same geostrophic balance as in (3). However, unlike the horizontal momentum equations, the vorticity equation (11a) is unaffected by $\bar{\eta}$ when the divergence equals zero and can therefore be solved for any $\bar{u}(\phi)$.

2.2.2. Linear perturbations

To first-order with respect to the decomposition (2) the ND model reduces to

$$\frac{\partial\zeta'}{\partial t} + \frac{\bar{u}}{a\cos\phi}\frac{\partial\zeta'}{\partial\lambda} + \frac{v'}{a}\frac{d}{d\phi}(\bar{\zeta} + f) = 0, \tag{13a}$$

$$\boldsymbol{k}\cdot\boldsymbol{\nabla} \times \left[(\bar{\zeta} + f)\boldsymbol{u}' + \zeta'\bar{\boldsymbol{u}}\right] - \nabla^2\left[\bar{\boldsymbol{u}}\cdot\boldsymbol{u}' + g\eta'\right] = 0. \tag{13b}$$

The number of unknowns in (13a) can be reduced to one by defining a stream function ψ as follows

$$\boldsymbol{u} = \boldsymbol{k} \times \boldsymbol{\nabla}\psi. \tag{14}$$

Using the relation $\zeta = \nabla^2\psi$, the vorticity equation in terms of ψ is

$$\left(\frac{\partial}{\partial t} + \frac{\bar{u}}{a\cos\phi}\frac{\partial}{\partial\lambda}\right)\left[\frac{1}{a\cos^2\phi}\frac{\partial^2\psi'}{\partial\lambda^2} + \frac{1}{a\cos\phi}\frac{\partial}{\partial\phi}\left(\cos\phi\frac{\partial\psi'}{\partial\phi}\right)\right]$$
$$+ \frac{1}{a\cos\phi}\frac{\partial\psi'}{\partial\lambda}\frac{d}{d\phi}(\bar{\zeta} + f) = 0. \tag{15}$$

Seeking a zonally propagating wave solution of the form $\psi' = \hat{\psi}(\phi)\exp[i(k\lambda - \omega t)]$ yields

$$(\omega - \bar{\omega})\frac{d^2\hat{\psi}}{d\phi^2} - (\omega - \bar{\omega})\tan\phi\frac{d\hat{\psi}}{d\phi} - \left[(\omega - \bar{\omega})\frac{k^2}{\cos^2\phi} + \frac{k}{\cos\phi}\frac{d}{d\phi}(\bar{\zeta} + f)\right]\hat{\psi} = 0, \tag{16}$$

where $\bar{\omega} = \bar{u}(a\cos\phi)^{-1}$ is the angular velocity of the mean flow. This equation is identical to equation (3) of Hartmann (1983).

2.3. The quasi-geostrophic system

For the QG model we use the equation derived in Schubert *et al.* (2009) (their equation (2.12)), which in our notation reads

$$\left(\frac{\partial}{\partial t} - \frac{1}{a^2 \cos \phi} \frac{\partial \psi}{\partial \phi} \frac{\partial}{\partial \lambda} + \frac{1}{a^2 \cos \phi} \frac{\partial \psi}{\partial \lambda} \frac{\partial}{\partial \phi} \right)$$

$$\times \left[\frac{1}{a^2 \cos^2 \phi} \frac{\partial^2 \psi}{\partial \lambda^2} + \frac{1}{a^2 \cos \phi} \frac{\partial}{\partial \phi} \left(\cos \phi \frac{\partial \psi}{\partial \phi} \right) - \frac{(2\Omega)^2}{gH} \sin^2 \phi \, \psi + 2\Omega \sin \phi \right] = 0, \quad (17)$$

where, again, the definition of the stream function ψ is the same as in the ND model in (14). Substituting $\psi = \bar{\psi}(\phi) + \psi'(\lambda, \phi, t)$, using the definition of ψ to replace $\partial \bar{\psi}/\partial \phi$ with $\bar{u}$, and using the relation $gh = 2\Omega \sin \phi \psi$, established within the QG assumptions, to replace $\bar{\psi}(\phi)$ with $\bar{\eta}(\phi)$ yields the following equation for the linear response

$$\left(\frac{\partial}{\partial t} - \frac{1}{a^2 \cos \phi} \frac{\partial \bar{\psi}}{\partial \phi} \frac{\partial}{\partial \lambda} \right)$$

$$\times \left[\frac{1}{a^2 \cos^2 \phi} \frac{\partial^2 \psi'}{\partial \lambda^2} + \frac{1}{a^2 \cos \phi} \frac{\partial}{\partial \phi} \left(\cos \phi \frac{\partial \psi'}{\partial \phi} \right) - \frac{(2\Omega)^2}{gH} \sin^2 \phi \, \psi' \right]$$

$$+ \left(\frac{1}{a^2 \cos \phi} \frac{\partial \psi'}{\partial \lambda} \frac{\partial}{\partial \phi} \right)$$

$$\times \left[\frac{1}{a^2 \cos \phi} \frac{\partial}{\partial \phi} \left(\cos \phi \frac{\partial \bar{\psi}}{\partial \phi} \right) - \frac{(2\Omega)^2}{gH} \sin^2 \phi \, \bar{\psi} + 2\Omega \sin \phi \right] = 0. \quad (18)$$

Seeking zonally propagating wave solutions of the form $\psi' = \hat{\psi}(\phi) \exp[i(k\lambda - \omega t)]$ yields

$$(\omega - \bar{\omega}) \frac{d^2 \hat{\psi}}{d\phi^2} (\omega - \bar{\omega}) \tan \phi \frac{d\hat{\psi}}{d\phi}$$

$$- \left[(\omega - \bar{\omega}) \frac{k^2}{\cos^2 \phi} + \frac{k}{\cos \phi} \frac{d}{d\phi} (\bar{\zeta} + f) - \omega \frac{(2\Omega a)^2}{gH} \sin^2 \phi + \frac{2k(2\Omega)}{H} \bar{\eta} \right] \hat{\psi} = 0. \quad (19)$$

This equation is identical to the ND system in equation (16), except for the last two terms in the square brackets. For finite $\bar{\eta}$, these two terms vanish as $1/H \to 0$, so the resulting QG system is expected to converge to those of the non-divergent system in this limit.

2.4. Methods of solution

In section 4 we solve equations (8), (16) and (19) in order to compare the growth rates obtained using the SWEs, ND and QG systems of equations in response to the basic-state in (24). In order to solve these equations we use the Chebyshev collocation method in which the derivatives are replaced by a Chebyshev differentiation matrix and the resulting (algebraic) eigenvalue problem is solved to find the eigenvalues (frequencies) and eigenfunctions (meridional structure) (see, e.g. Trefethen 2000). The Chebyshev collocation method was successfully applied to rotating shallow water equations for both real (e.g. De-Leon and Paldor 2011, Paldor *et al.* 2013) and imaginary (e.g. Ribstein *et al.* 2014) eigenvalue problems. This method yields a plethora of normal modes all at once and can

therefore be used to sweep through different parameters values and perform sensitivity tests. In order to validate the results we repeat a subset of the calculations using the shooting-to-a-fitting-point method in which the equations are integrated from the singular poles starting with the regular solutions into an arbitrary matching point (taken here to be $\phi = 0.1$ radians) where the solutions are required to be continuous (see, e.g. Press *et al.* 1992). For the SWEs the shooting method is applied to system (9) instead of (8). The shooting method was successfully employed in a variety of instability studies in GFD problems (e.g. Killworth *et al.* 1984, Cohen *et al.* 2016).

3. General considerations of the approximation of SWEs by the QG and ND systems

The SWEs are Euler equations of fluid mechanics in a thin layer where the horizontal velocity is independent of height when the Coriolis force is added to the pressure-gradient force in driving the temporal changes in velocity. In contrast, the QG and ND equations are simplifications of the basic SWEs system that approximate the fluid dynamics in some limits e.g. small Rossby number and/or low frequency (Vallis 2006, Pedlosky 2013). In this section we examine the intricate relationships between these three systems using coordinate free forms of the equations and identify the ranges of parameters where solutions of the QG and ND equations can be expected to yield acceptable approximations to solutions of the SWEs. Our approach follows that employed in Paldor (2008) in the study of the relation between Rossby wave solutions in the SWEs and the ND systems. To simplify the analysis the examination is carried out on the free linearised systems which is the most widely employed set-up in analytic theories.

Using the notation employed above the vectorial form of the linearised SWEs (where velocity is linearised about 0 and height deviation about a mean constant height H) is

$$\frac{\partial \boldsymbol{u}}{\partial t} = -f\boldsymbol{k} \times \boldsymbol{u} - g\nabla\eta, \tag{20a}$$

$$\frac{\partial \eta}{\partial t} = -H\nabla\cdot\boldsymbol{u}, \tag{20b}$$

where again, $\boldsymbol{u} = (u, v)$ is the horizontal velocity vector, η is the free surface height anomaly with respect to H, $f = 2\Omega \sin\phi$ is the Coriolis parameter, g is the gravitational acceleration, and $\boldsymbol{k}$ is the unit vector in the vertical direction.

Application of the $\boldsymbol{k}\cdot\nabla\times$ and $\nabla\cdot$ operators on the momentum equation yields two scalar equations for the vorticity, $\zeta = \boldsymbol{k}\cdot\nabla\times\boldsymbol{u}$, and the divergence, $\delta = \nabla\cdot\boldsymbol{u}$ (and modifies the height deviation, η). They are

$$\frac{\partial \zeta}{\partial t} + f\delta + \beta v = 0, \tag{21a}$$

$$\frac{\partial \delta}{\partial t} + f\zeta + \beta u + g\nabla^2\eta = 0, \tag{21b}$$

$$\frac{\partial \eta}{\partial t} + H\delta = 0, \tag{21c}$$

where β is the rate of change of Coriolis parameter with latitude (i.e. in Cartesian coordinates $f = f_0 + \beta y$). No assumption was made in deriving this (ζ, δ, η) system so its

solutions are identical to those of the original linearised SWEs (20). The assumptions imposed on this set in order to derive the approximate ND and QG systems are detailed next.

ND: The assumption of non-divergence implies that $\delta = 0$ has to be substituted in system (21). Under this assumption, the continuity equation (21c) implies that $\partial\eta/\partial t = 0$ while the vorticity equation (21a) implies $\partial\zeta/\partial t = -\beta v$. The latter condition, $\partial\zeta/\partial t = -\beta v$, implies that v is time-dependent and therefore so must be u. Setting $\delta = 0$ in the divergence equation (21b) and considering the time dependence of ζ and u and the time-independence of η then yields a diagnostic equation in which $f\zeta + \beta u$ is time-dependent while $g\nabla^2\eta$ is independent of time. The implications of this unusual diagnostic relation are ignored in ND theories. However, regardless of these implications, for not-too-fast time variations, i.e. when $\partial/\partial t = \mathrm{O}(1)$, the continuity equation implies $\delta = \mathrm{O}(H^{-1})$ so the ND solutions can be expected to provide acceptable approximations to solutions of the SWEs at large values of H.

QG: A key assumption in the formulation of the QG equation is that the system is "near" the steady geostrophic balance which is non-divergent only on the f-plane. Though the slow time variation is only one of several additional approximations that have to be imposed to fully justify the QG approximation (Vallis 2006, Pedlosky 2013) its application to SWEs implies that while the velocity and η variables, as well as the parameters, are $\mathrm{O}(1)$, time variations are, in some sense, small, i.e.

$$\frac{\partial}{\partial t} = \mathrm{O}(\epsilon), \qquad \text{where} \quad \epsilon \ll 1. \qquad (22)$$

(The small parameter ϵ can be thought of as the absolute value of the frequency.)

Under the low frequency assumption (while H is $\mathrm{O}(1)$) the continuity equation implies that

$$\frac{\delta}{\eta} = \frac{-\epsilon}{H} = \mathrm{O}(\epsilon) \ll 1. \qquad (23)$$

Accordingly, the first two terms on the left-hand side of the vorticity equation, $\partial\zeta/\partial t$ and $f\delta$, are both $\mathrm{O}(\epsilon)$ so for consistency, on the β-plane, the third term, βv, must also be $\mathrm{O}(\epsilon)$. This limitation, which is commonly employed in traditional derivations of the QG system, limits the approximation of the SWEs by the QG system to small meridional velocity (or domain). The $\mathrm{O}(1)$ terms in the divergence equation, $f_0\zeta + g\nabla^2\eta$, simply reflect the non-divergent geostrophic balance on the f-plane about which the QG approximation is constructed while the $\beta(\zeta y + u)$ terms are the $\mathrm{O}(\epsilon)$ correction to this balance. The time dependent, $\partial\delta/\partial t$, term is $\mathrm{O}(\epsilon^2)$ only. Clearly, (23) implies that for fixed ϵ, $\delta \to 0$ in the limit when $H^{-1} \to 0$ so, as is found in the ND equation, solutions of the QG equation should also provide an accurate approximation of solutions of the SWEs only at large H.

Having established that solutions of both ND and QG equations can be expected to accurately approximate the primordial SWEs at large values of H there are three questions that need to be addressed:

(i) Is this expectation verified by numerical solutions in a particular set-up?
(ii) Are the values of H where each of the ND and QG solutions approximate the SWEs solutions identical/similar?
(iii) How do the values of H where the ND and QG solutions approximate the SWEs compare with values of the realistic atmosphere/ocean.

In the next section we calculate the linear instabilities of a zonal jet on a sphere using the QG and SWEs systems and compare these instabilities to instabilities that were calculated in the 1980s using the ND equations.

4. Results

The particular set-up employed here to examine the relation between the ND, QG and SWEs systems is the linear instability of a zonal jet on a sphere. This problem was already analyzed in the ND system by Hartmann (1983) for polar jets. Here we extend the calculation to the QG and SWEs systems and consider both polar (section 4.1) and equatorial (section 4.2) jets. We choose these cases to test the difference between the three systems since the limitations of the ND and QG equations are most applicable for strong jets, and the shear of the wind surrounding a strong jet can lead to a reversal of the mean potential vorticity gradient and hence to barotropic instability. Specifically, the analytic wind profile used in Hartmann (1983) that provides a convenient base of comparison between the three systems is given by

$$\bar{u}(\phi) \; = \; u_0 \text{sech}[2(\phi - \phi_0)/B] \cos \phi, \tag{24}$$

where u_0, ϕ_0 and B are free parameters that characterise the chosen jet's amplitude, central latitude and width, respectively. A consistent specification of the basic-state requires also that $0 \leq \bar{h} = H + \bar{\eta}$ (where $\bar{\eta}$ is given by (4) and (5)) at all ϕ. This condition restricts the values of u_0, ϕ_0 and B. Figure 1 presents contour plots of the global minimum over all latitudes of $\bar{h}$ (i.e. $\min_\phi \bar{h}$) in geostrophic balance with the zonal wind in (24) for different ranges of u_0, ϕ_0 and B. Indeed, it can be seen that for reasonable values of the parameters considered in Hartmann (1983) the imposition of the spherical geostrophy relation between $\bar{\eta}$ and $\bar{u}$ leads to negative $\min_\phi \bar{h}$ for some values of H between 1 and 6 km.

4.1. Polar jets

We begin the comparison between the SWEs, ND and QG systems by exploring the sensitivity of the growth rates of barotropic instability of linear perturbations on the zonal mean jet of (24) to the layer depth (H in (2c)). Figure 2(a) shows the growth rates of the most unstable mode as a function of H for zonal wavenumber 1 for a mean wind profile with $u_0 = 180$ m/sec, $\phi_0 = 60°$ and $B = 10°$ in equation (24). We choose these parameter values in order to compare our results with those of the non-divergent model employed in Hartmann (1983). Note that for the meridional structure in (24), the maximal wind of the jet for the above values is 91 m/sec, a speed similar to that observed in the Southern Hemisphere upper stratosphere. For values of H smaller than about 2 km (2032 m), the height field $\bar{h}$ in geostrophic balance with the strong zonal wind is negative at the North Pole (i.e. $\bar{\eta} < -H$ there), and hence the basic state is unphysical (see section 2.1). For layer depths slightly
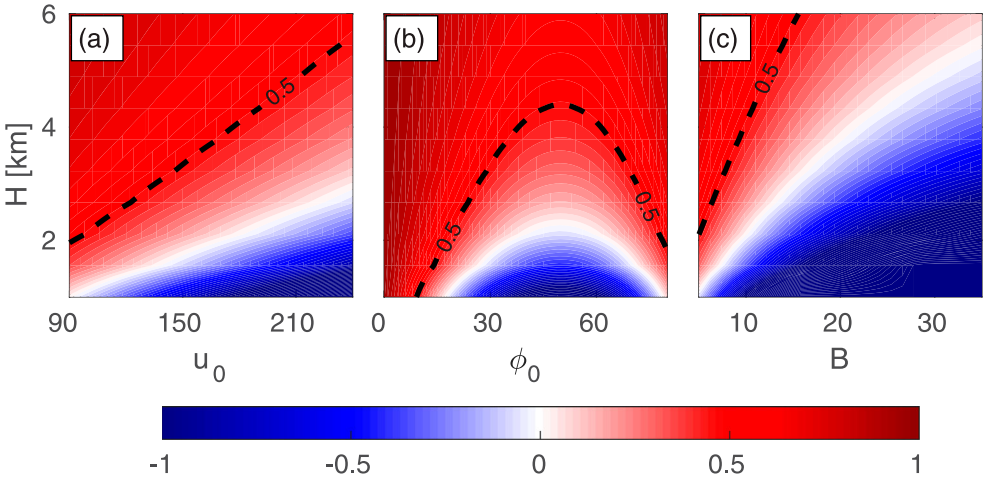
Figure 1. Minimum over all latitudes of the normalised mean height profile (i.e. $\min_\phi \bar{h}/H$) in (spherical) geostrophic balance with the zonal wind specified in equation (24). Red-shaded, white-shaded and blue-shaded contours correspond to positive, zero and negative values of $\min_\phi \bar{h}/H$. Accordingly a value of $\min_\phi \bar{h}/H = +0.25$, for example, is indicated by a light red colour. In practice, it is unlikely that the value of $\bar{h}$ would deviate from H by more than 50%. Thus, the 0.5 contour is indicated by a black dashed lines in order to mark the feasible regions of the parameters (above the 0.5 contour). Note, that formally $\min_\phi \bar{h}/H$ is bounded from above by 1 and unbounded from below so the lower contour range in this figure was set to -1 arbitrarily. The contours are shown on planes where the ordinate is H (in the range $1 \leq H \leq 6$ km) and the abscissa is one of the following zonal jet parameters: (a) u_0 for $\phi_0 = 60°$ and $B = 10°$. (b) ϕ_0 for $u_0 = 180$ m sec^{-1} and $B = 10°$. (c) B for $u_0 = 180$ m sec^{-1} and $\phi_0 = 60°$ (colour online).

larger than this threshold, the growth rate of instabilities in the SWEs (shown in blue and black dots for the two numerical methods) is at least an order of magnitude smaller than the growth rate in the ND system (dashed red line). Likewise, for layer depths slightly larger than the threshold the growth rates in the QG system are significantly smaller than those of the ND system, but are somewhat larger than the growth rates in the SWEs. At layer depths that are an order of magnitude larger (e.g. 30 km) there is little difference between the growth rates in the three systems, which is consistent with the convergence of the equations for the three systems in the limit $1/H \to 0$. Hence the depth of the layer is a crucial parameter for approximating the growth rate of the SWEs system by either the ND or the QG systems, but this limitation is completely ignored in the solution of the ND system that has no height perturbations whatsoever. Results are similar for zonal wavenumbers 2 and 3 shown in the panels (b) and (c) of figure 2: only for a layer depth that exceeds 10 km do the results of the ND system agree to within 20%, and only at depths larger than 30 km (i.e. exceeding the thickness of the ocean or the Troposphere) the differences can be considered negligible.

The growth rates of the jet in the SWEs in panels (a) and (b) of figure 2 appear to reach a cut-off at about $H = 3$–5 km, below which the growth rates become zero and the jet becomes stable. Usually this transition occurs in the form of a bifurcation where two stable wave-modes coalesce in the $\omega_r - k$ plane and an unstable mode appears in the $\omega_i - k$ (as a conjugate pair). As indicated by the lack of black dots in the vicinity of these potential
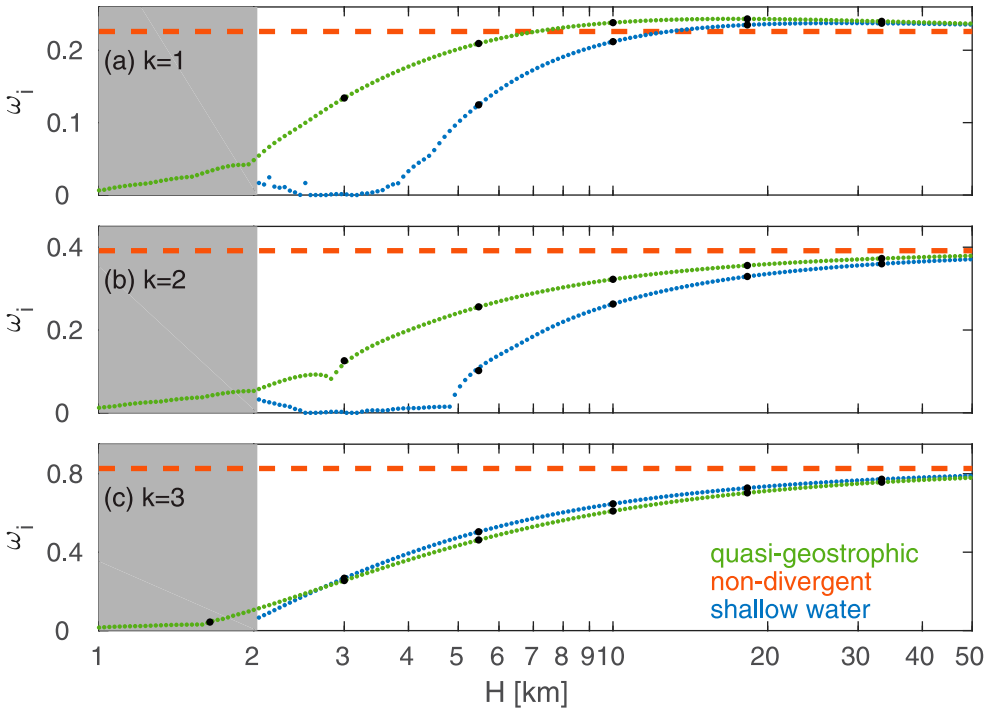
Figure 2. Growth rate (in units of 1/day) of the most unstable mode of the zonal wind specified in (24) with $u_0 = 180$ m/sec, $\phi_0 = 60°$ and $B = 10°$ as a function of H for $k = 1, 2, 3$ panels (a), (b), (c), respectively. Note that for the meridional structure in (24), the maximal wind of the jet for the above values is only 91 m/sec. The gray shaded portion corresponds to values of H for which $\min_\phi \bar{h} \leq 0$. Blue dots: growth rates of the shallow water model obtained using the Chebyshev collocation method. Red dashed line: growth rate of the non-divergent model. Green dots: growth rates of the QG model obtained using the Chebyshev collocation method. Black dots: growth rates obtained using the shooting method (colour online).

bifurcations, our numerical calculations are insufficiently accurate to describe these transitions smoothly. However, these considerations are beyond the scope of the present work that focuses on the difference between the three systems and not a full fledged stability analysis.

Though the growth rates of the most unstable modes are substantially smaller in the shallow water and QG systems, the structure of the most unstable mode differs only slightly in the three systems. Figure 3 shows the structure of the most unstable mode of the zonal wind specified in (24) with $u_0 = 180$ m/sec, $\phi_0 = 60°$, $B = 15°$ and zonal wavenumber 1, obtained using the SWEs (a) and (d), the QG system (b) and (e) and the ND system (c) and (f). The solutions of the shallow water and QG system are shown for $H = 10$ km. In all solutions the fields' amplitudes are normalised on $\max_\phi |\hat{v}|$ in order to provide a consistent baseline for comparison. Even though the structure of the wind fields are qualitatively similar, the magnitude of the zonal wind component is stronger in the QG and SWEs systems.

Having demonstrated the differences in the resulting growth rates between the three system, and shown that they belong to the same unstable mode, we now examine the
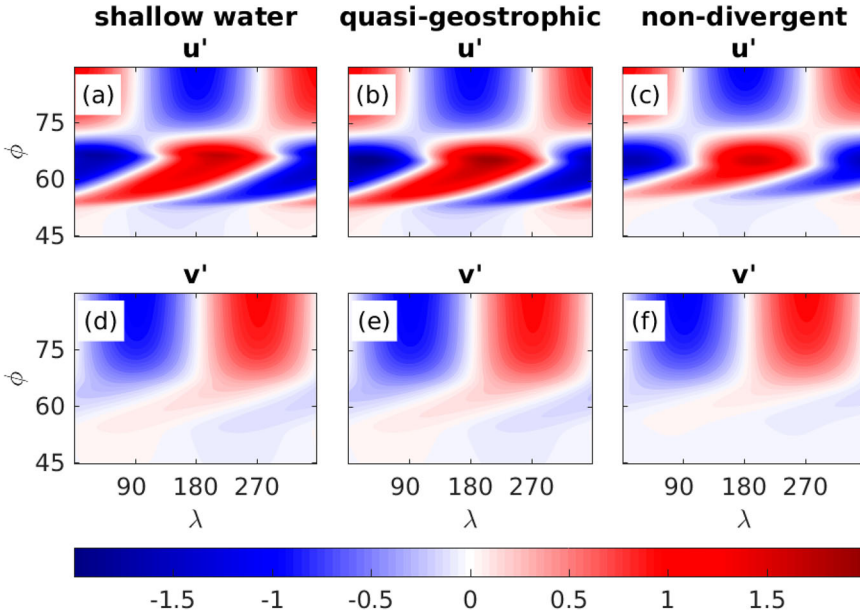
Figure 3. Latitude–longitude maps u' and v' of most unstable mode of the zonal wind specified in (24) with $u_0 = 180$ m/sec, $\phi_0 = 60°$ and $B = 10°$, obtained using the SWEs (a,d), the QG system (b,e) and the ND system (c,f). The solutions of the shallow water and QG system are shown for $H = 10$ km. In all solutions the fields' amplitudes are normalised on $\max_\phi |\hat{v}|$ in order to provide a consistent baseline for comparison (colour online).

sensitivity of the above differences to the three parameters governing the zonal wind profile. Figure 4 shows the growth rates of the most unstable mode for $k = 2$ as a function of the jet's magnitude u_0 (a), its peak latitude ϕ_0 (b) and its width B (c), obtained using the ND (red), QG (green) and SWEs (blue) systems. In all cases, the growth rates are lowest in the SWEs system and highest in the ND system, and can be as large as 90% different (for $B = 15°$). For wavenumber 1, the growth rates of the QG model become larger than the ND system as the jet strengthens.

4.2. Equatorial jets

In the previous section we demonstrated the difference between the SWEs, QG and ND systems in terms of the linear stability of a polar jets. However, the results can be rather different for equatorial jets. Most notably, the mean height profile in geostrophic balance with an equatorial jet decays over a shorter interval, and hence the requirement $\bar{h} \geq 0$ is less restrictive. Indeed, as indicated by figure 1, for $u_0 = 180$ m/sec, $B = 10°$ and $\phi_0 = 0$, $\min_\phi \bar{h}/H$ remains positive for all values of H between 1 to 6 kilometers. Thus in this section we repeat the analysis of section 4.1 for $\phi_0 = 0$.

Figure 5 shows the growth rates of the most unstable mode as a function of H for the same zonal wind profile as in figure 2 with $u_0 = 180$ m/sec and $B = 10°$ but $\phi_0 = 0°$. For $\phi_0 = 0$, the maximal wind of the jet in (24) equals u_0. Thus, the maximal wind of the jet in figure 5 equals 180 m/sec. Despite the stronger winds of the jet in this case, compared to the polar jet in figure 2, the height field in geostrophic balance with the zonal jet remains
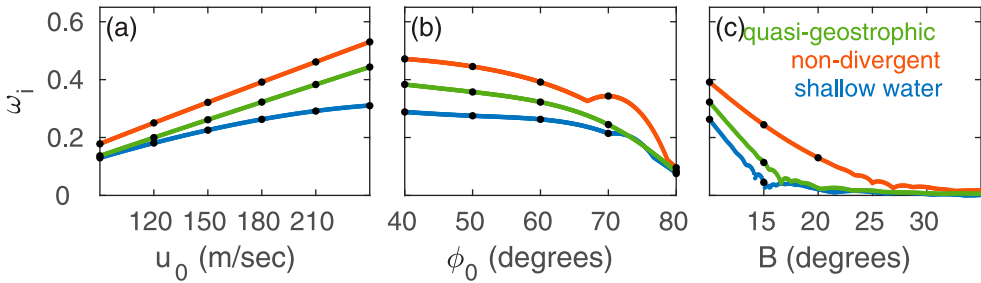
Figure 4. Growth rates sensitivity to changes in the zonal wind parameters u_0 (a), ϕ_0 (b) and B (c) for wavenumber $k = 2$. (a) while holding $\phi_0 = 60°$ and $B = 10°$ fixed. (b) while holding $u_0 = 180$ m/sec and $B = 10°$ fixed. (c) while holding $u_0 = 180$ m/sec and $\phi_0 = 60°$ fixed. Blue: shallow water model with $H = 10$ km. Red: non-divergent model. Green: quasi-geostrophic model with $H = 10$ km. Black dots: growth rates obtained using the shooting method (colour online).
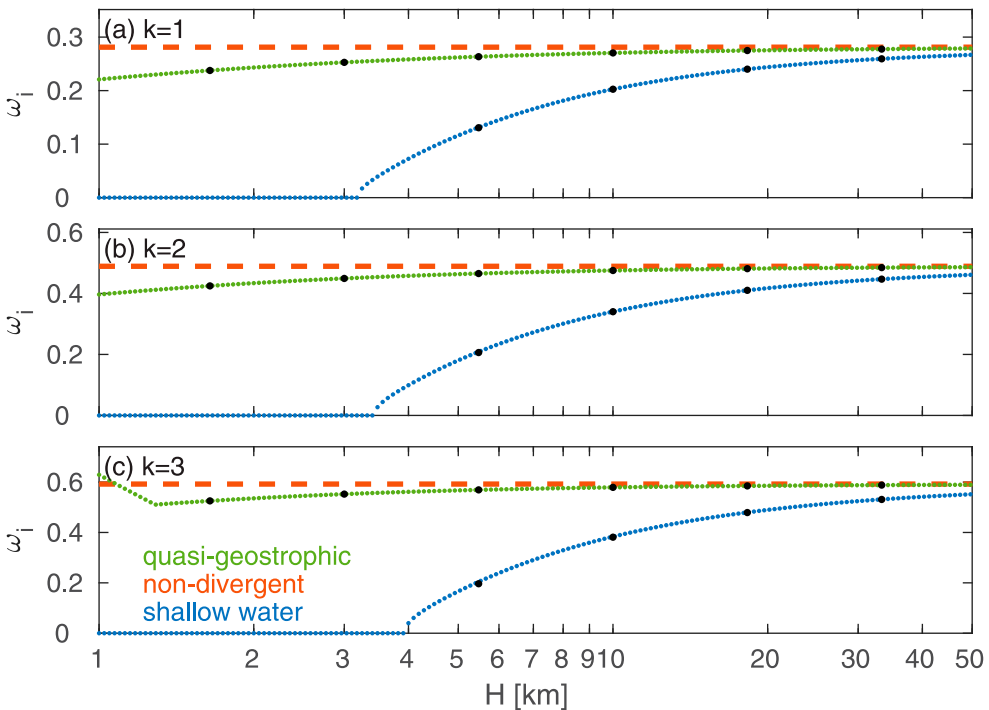

Figure 5. Same as figure 2, but for $\phi_0 = 0$ (colour online).

positive at all latitudes for all values of H down to 1 km. Furthermore, despite the stronger winds of the jet in this case, the growth rates are generally similar to those of the polar jet in figure 2. However, the differences between the SWEs and its ND and QG approximate system are more pronounced in this case even though, as in the case of the polar jet in figure 2, the differences between the three systems approach zero with the increase in the layer depth. Specifically, in the SWEs system the jet becomes stable for layer depths of

between 3 and 4 km, while in the ND and QG systems the jet remains unstable for layer depths down to 1 km. For layer depths of around 10–15 km (i.e. approximately the depth of similar-signed zonal winds associated with the Quasi-Biennial Oscillation), the growth rates for the SWE are around 3/4 of that for the ND and QG approximate systems. Furthermore, as opposed to the polar jet, where the QG approximation is closer to the SWEs, in the equatorial jet the QG approximation is closer to the ND approximation. This result can be expected considering the fact that the geostrophic balance becomes less accurate in the vicinity of the equator (since the rate of change of $\sin\phi$ is fastest at small ϕ). Hence, for equatorial jets, the QG equation provides accurate approximation of the SWEs only for large values of H where the ND equation provides accurate approximation of the SWEs. With regard to the validity of the approximation in the vicinity of the equator it should also be noted that all three systems considered in this work neglect the contribution of the Coriolis force due to vertical motions. In the primitive equations, this contribution appears as $w\cos\phi$ in the u-momentum equation (with a plus sign when written on the left-hand side of the equation), where w is the vertical velocity. Clearly, at the equator this term cannot be neglected compared to the $v\sin\phi$ (with a minus sign when written on the left-hand side of the equation) contribution of the Coriolis force, regardless of the magnitudes of v and w. Recently, it has been recognised that the inclusion of the this term can influence the properties and stability of the equatorial jets (Gerkema *et al.* 2008), and a system of SWEs accounting for this term has been derived (Tort *et al.* 2014). However, in the present work we are concerned with the differences between the SWEs and the QG and ND approximations and, therefore, consider these systems in their 'traditional' forms.

Figure 6 shows the structure of the most unstable mode of the zonal wind specified in (24) with $u_0 = 180$ m/sec, $\phi_0 = 0°$, $B = 15°$ and zonal wavenumber 1, obtained using the SWEs (a) and (d), the QG system (b) and (e) and the ND system (c) and (f). The solutions of the shallow water and QG system are shown for $H = 10$ km. In all solutions the fields' amplitudes are normalised on $\max_\phi |\hat{v}|$ in order to provide a consistent baseline for comparison. As in the case of the polar jet, the structure of the most unstable mode in all three systems corresponds to the same mode. However, unlike the polar jet where the maximal zonal wind in the mid-latitudes was about twice larger than the maximal meridional wind, in the equatorial jet the maximal zonal wind in the vicinity of the equator is about 10 times larger than the maximal meridional wind.

Figure 7 shows the growth rates of the most unstable mode for $k = 2$ as a function of the jet's magnitude u_0 (a), its peak latitude ϕ_0 (b) and its width B (c), obtained using the ND (red), QG (green) and SWEs (blue) systems. Considering panel (b) of this figure, it seems that the growth rates in the SWEs and ND are almost independent of ϕ_0 between $0°$ and $40°$, and that the QG approximation is closer to the ND approximation than to the SWEs for ϕ_0 between $0°$ and $30°$. Wider tropical jets are more stable (figure 7(c)) for all three systems, but are most stable for the SWEs system regardless of the width.

5. Summary and discussion

The effects of divergence on the growth rates of barotropic instabilities are studied by examining the linear stability of both a strong polar jet and a strong equatorial one and comparing the growth rates obtained from the Shallow Water Equations (SWEs) with those
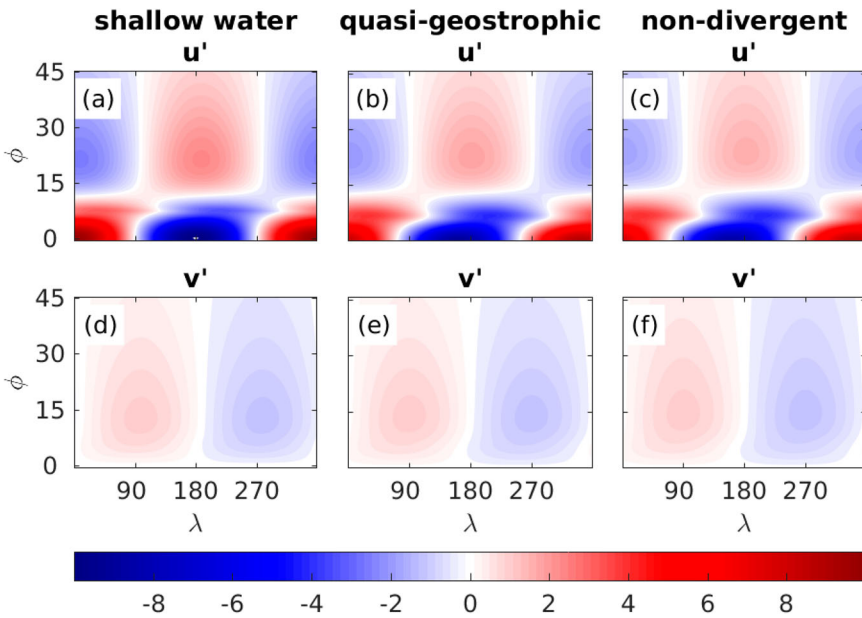
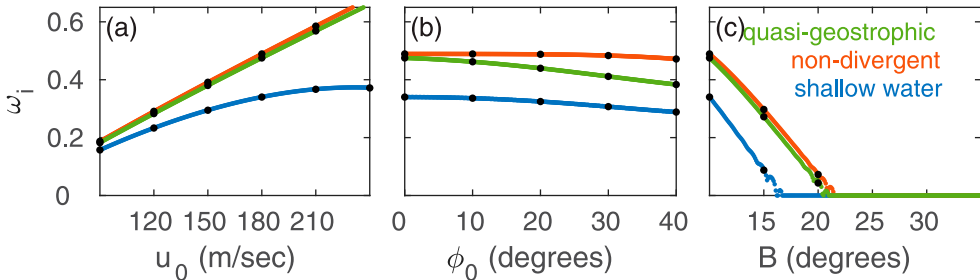**Figure 6.** Same as figure 3, but for $\phi_0 = 0$ (colour online).

Figure 7. Same as figure 4, but for $\phi_0 = 0$ in panels (a) and (c) and ϕ_0 spanning the interval $0°$ to $40°$ in panel (b) (colour online).

from the non-divergent barotropic vorticity (ND) equation and the QG vorticity equation. We choose these test cases for two reasons:

(i) The limitations of the ND system are most applicable for strong jets.
(ii) Meridional gradients of speed in strong zonal jets can lead to a reversal of the potential vorticity gradient making the jets susceptible to barotropic instability.

The shallow water equations can be related back to the primitive equations if the temperature and wind profiles are sufficiently simple or if a specific atmospheric layer is chosen (Zeitlin 2018), and hence this system employs the least number of approximations of the three systems. The non-divergent system, on the other hand, assumes non-divergence which severely limits its accuracy.

In terms of growth rates, the effects of divergence depend on the chosen depth H (that determines the layer depth in a motionless basic state), with smaller H generally leading to smaller growth rates. Depending on the specific application or the interpretation assigned to it, this parameter can vary by several orders of magnitude. The shallow water depth of the barotropic mode, for example, can be interpreted as either the 'entire column' depth, which is about 30 km for the stratosphere, or as the 'equivalent height' of the barotropic mode in a multi-layer model, which is only about 5–10 km (De-Leon *et al.* 2020). In baroclinic cases, the equivalent depth in the atmosphere was shown to be on the order of 100 m (Wheeler and Kiladis 1999, Kiladis *et al.* 2009, De-Leon *et al.* 2020). By examining the stability of the mean zonal wind profiles as a function of H it is found that for $H \geq 30$ km the non-divergent system may provide a sufficiently good approximation. However for H between 5 and 10 km the growth rates of the shallow water system can be more than 50% smaller than those of the non-divergent model. This result is consistent with that of Paldor and Dvorkin (2006), who compared the instabilities arising from a Kuo type cosine jet in a channel obtained using the non-divergent vorticity equation with those obtained using the SWEs. As was found in this study, they too show that for realistic values of the ocean depth the maximal growth rates are smaller in the SWEs than in the former. Thus, the importance of divergence to the growth rates of barotropic instabilities of strong polar jets depends on the specific application and the relevant value of H. The similarity of the growth rates for large H is consistent with theoretical expectations, though the specific convergence of the growth rates for $H \geq 30$ km cannot be predicted from analytic considerations in the absence of numerical results.

Is linear growth of barotropic instability relevant for the stratosphere? The Potential Vorticity (PV) gradient on the poleward flank of the Southern Hemisphere vortex reverses for up to half the time during austral winter, and occasionally reverses for several consecutive days (Rodas and Pulido 2017). We have examined the growth rates for the stratospheric jet during the period July 11 through 15 2008 (a period considered in section 3.2 of Rodas and Pulido 2017), and found values of ω_i that are generally similar to those shown here for the idealised jet profile (details not shown). The values of ω_i approach 1 day^{-1} even for depths less than 10 km, and hence over the course of 4 days any pre-existing perturbation can grow by more than 400%. That being said, instability depends not only on the depth of the layer over which the PV gradient is reversed, but also upon the rate at which the PV reversal is restored by other processes as the resulting instability removes the reversal. The relevance of the instability also depends on the asymmetry of the jet, as the zonal average may obscure the fact that the PV gradient may be strongly reversed on one side of the vortex and not the other. The nonlinear growth of perturbations may differ from the linear growth of perturbations if finite amplitude effects become important. Finally, the polar vortex may also become baroclinically unstable in the lower mesosphere, and this baroclinic instability may enhance growth rates. Several studies have noted the possibility that the westerly phase of the Quasi-Biennial Oscillation may feature barotropic instability in the subtropical shear zone (Shuckburgh *et al.* 2001, Hitchman and Huesmann 2009, Garcia and Richter 2019). For layer depths of 10 km, the growth rate of barotropic instability of an identical equatorial jet is around 25% smaller in the SWE system than in the ND and QG systems (figure 7). In all cases e-folding timescales are between 1 and 5 days, and hence in monthly mean data one should expect signatures of barotropic instability if the mean state potential vorticity gradient reverses.

While we have focused on the barotropic instability of Earthly jets, our results might also be applicable to other planets such as Venus where barotropic instability is believed to play a role in supporting supperrotation (Sánchez-Lavega *et al.* 2017, Read and Lebonnois 2018). In considering this possibility it is necessary to consider the planet's physical parameters, i.e. its mean radius, gravitational acceleration and angular frequency, in addition to the layer's depth. In fact, if the system is non-dimensionalised as in Paldor *et al.* (2013) the only non-dimensional parameter, excluding the basic state parameters, is $\alpha = gH/(2\Omega a)^2$. Following the arguments of section 3, it follows that the three systems converge in the limit of large α, so that the large H limit considered here is also relevant if a or Ω are small. In Venus' case, its mean radius and gravitational acceleration are of the same order of Earth's, but its angular frequency is about 2 orders of magnitude smaller. Thus, for the same range of layer depths considered here α on Venus is 4 orders of magnitude larger than on Earth, so the results of the present study suggest that the ND and QG approximations might be more reasonable on Venus than on Earth. On the other hand, on the equator, the $w \cos \phi$ contribution of the Coriolis force to the u-momentum equation cannot be neglected and (as discussed in Gerkema *et al.* 2008, Tort *et al.* 2014) its inclusion can influence the stability properties of the jets.

Overall this study clarifies the effects of the system of equations chosen has on barotropic instability. We find that the non-divergent system overestimates growth rates, and this overestimation is particularly acute if the depth of the barotropically unstable layer is small.

Disclosure statement

No potential conflict of interest was reported by the authors.

Funding

ORCID

Nathan Paldor 🔟 http://orcid.org/0000-0002-4419-4201

References

Andrews, D.G., Leovy, C.B. and Holton, J.R., *Middle Atmosphere Dynamics*, 40, 1987. (Orlando, FL: Academic Press).

Chapman, S. and Lindzen, R., *Atmospheric Tides*, 200 pp., 1970. (D. Reidel: Norwell Mass).

Cho, J.Y.K. and Polvani, L.M., The emergence of jets and vortices in freely evolving, shallow-water turbulence on a sphere. *Phys. Fluids* 1996, **8**, 1531–1552.

Cohen, Y., Dvorkin, Y. and Paldor, N., On the stability of outcropping eddies in a constant-PV ocean. *Q. J. Roy. Meteor. Soc.* 2016, **142**, 1920–1928.

De-Leon, Y., Grafinkel, C.I. and Paldor, N., Barotropic modes, baroclinic modes and equivalent depths in the atmosphere. *Q. J. Roy. Meteor. Soc.* 2020, in submission.

De-Leon, Y. and Paldor, N., Zonally propagating wave solutions of Laplace tidal equations in a baroclinic ocean of an aqua-planet. *Tellus A* 2011, **63**, 348–353.

Garcia, R.R. and Richter, J.H., On the momentum budget of the quasi-biennial oscillation in the whole atmosphere community climate model. *J. Atmos. Sci.* 2019, **76**, 69–87.

Gerkema, T., Zimmerman, J., Maas, L. and Van Haren, H., Geophysical and astrophysical fluid dynamics beyond the traditional approximation. *Rev. Geophys.* 2008, **46**.

Gill, A.E., *Atmosphere-Ocean dynamics (International Geophysics Series)*, 1982. (San Diego, CA: Academic Press).

Hartmann, D.L., Barotropic instability of the polar night jet stream. *J. Atmos. Sci.* 1983, **40**, 817–835.

Hitchman, M.H. and Huesmann, A.S., Seasonal influence of the quasi-biennial oscillation on stratospheric jets and Rossby wave breaking. *J. Atmos. Sci.* 2009, **66**, 935–946.

Kiladis, G.N., Wheeler, M.C., Haertel, P.T., Straub, K.H. and Roundy, P.E., Convectively coupled equatorial waves. *Rev. Geophys.* 2009, **47**.

Killworth, P.D., Paldor, N. and Stern, M.E., Wave propagation and growth on a surface front in a two-layer geostrophic current. *J. Mar. Res.* 1984, **42**, 761–785.

Kuo, H.L., Dynamic instability of two-dimensional nondivergent flow in a barotropic atmosphere. *J. Meteorol.* 1949, **6**, 105–122.

Kuo, H.L., Dynamics of quasigeostrophic flows and instability theory. *Adv. Appl. Mech.* 1973, **13**, 247–330.

Paldor, N., Non-divergent 2D vorticity dynamics and the Shallow Water Equations on the rotating Earth, in *IUTAM Symposium on Hamiltonian Dynamics, Vortex Structures, Turbulence*, 2008, pp. 177–187.

Paldor, N., De-Leon, Y. and Shamir, O., Planetary (Rossby) waves and inertia–gravity (Poincaré) waves in a barotropic ocean over a sphere. *J. Fluid Mech.* 2013, **726**, 123–136.

Paldor, N. and Dvorkin, Y., Barotropic instability of a zonal jet: from nondivergent perturbations on the β plane to divergent perturbations on a sphere. *J. Phys. Oceanogr.* 2006, **36**, 2271–2282.

Pedlosky, J., *Geophysical Fluid Dynamics*, 2013. (New York, NY: Springer Science & Business Media).

Press, W., Teukolsky, S., Vetterling, W. and Flannery, B., *Numerical Recipes in Fortran 77: The Art of Scientific Computing*, pp. 933, 1992. (New York: Cambridge University Press).

Read, P.L. and Lebonnois, S., Superrotation on Venus, on Titan, and Elsewhere. *Annu. Rev. Earth Pl. Sc.* 2018, **46**, 175–202.

Reznik, G., Zeitlin, V. and Jelloul, M.B., Nonlinear theory of geostrophic adjustment. part 1. rotating shallow-water model. *J. Fluid Mech.* 2001, **445**, 93–120.

Ribstein, B., Zeitlin, V. and Tissier, A.S., Barotropic, baroclinic, and inertial instabilities of the easterly Gaussian jet on the equatorial β-plane in rotating shallow water model. *Phys. Fluids* 2014, **26**, 056605.

Rodas, C. and Pulido, M., A climatology of Rossby wave generation in the middle atmosphere of the Southern hemisphere from MERRA reanalysis. *J. Geophys. Res.-Atmos.* 2017, **122**, 8982–8997.

Rostami, M. and Zeitlin, V., Eastward-moving convection-enhanced modons in shallow water in the equatorial tangent plane. *Phys. Fluids* 2019, **31**, 021701.

Sánchez-Lavega, A., Lebonnois, S., Imamura, T., Read, P. and Luz, D., The atmospheric dynamics of venus. *Space Sci. Rev.* 2017, **212**, 1541–1616.

Schubert, W.H., Taft, R.K. and Silvers, L.G., Shallow water quasi-geostrophic theory on the sphere. *J. Adv. Model. Earth Sy.* 2009.

Shuckburgh, E., Norton, W., Iwi, A. and Haynes, P., Influence of the quasi-biennial oscillation on isentropic transport and mixing in the tropics and subtropics. *J. Geophys. Res.-Atmos.* 2001, **106**, 14327–14337.

Tort, M., Dubos, T., Bouchut, F. and Zeitlin, V., Consistent shallow-water equations on the rotating sphere with complete Coriolis force and topography. *J. Fluid Mech.* 2014, **748**, 789–821.

Trefethen, L.N., *Spectral Methods in MATLAB*, 10, 2000. (Philadelphia, PA: Siam).

Vallis, G.K., *Atmospheric and Oceanic Fluid Dynamics: Fundamentals and Large-scale Circulation*, 2006. (Cambridge, UK: Cambridge University Press).

Wheeler, M. and Kiladis, G.N., Convectively coupled equatorial waves: analysis of clouds and temperature in the wavenumber–frequency domain. *J. Atmos. Sci.* 1999, **56**, 374–399.

Zeitlin, V., *Geophysical Fluid Dynamics: Understanding (Almost) Everything with Rotating Shallow Water Models*, 2018. (Oxford, UK: Oxford University Press).

Appendix. Choice of reference mean height

In addition to the zonal wind, a complete determination of the basic-state requires also the specification of the mean height at a certain reference latitude. In the present work we found it convenient to use $\phi = -\pi/2$ (the south pole) as the point where the mean height is specified. In order to specify $\bar{\eta}(-\pi/2)$ in a meaningful way we further assume that the total mass (volume) in the layer (e.g. atmosphere or ocean) is unchanged by the mean zonal wind. Specifically, we assume that the layer's total mass (volume) equals its mass (volume) in a motionless basic state (i.e. when $\bar{u} = 0$), which implies

$$\int_0^{2\pi} \int_{-\pi/2}^{\pi/2} \int_a^{a+H+\bar{\eta}(\phi)} r^2 \cos\phi \, \mathrm{d}r \, \mathrm{d}\phi \, \mathrm{d}\lambda = \int_0^{2\pi} \int_{-\pi/2}^{\pi/2} \int_a^{a+H} r^2 \cos\phi \, \mathrm{d}r \, \mathrm{d}\phi \, \mathrm{d}\lambda. \tag{A1}$$

Carrying out the integrations yields

$$\int_{-\pi/2}^{\pi/2} \left[(a + H + \bar{\eta}(\phi))^3 - a^3 \right] \cos\phi \, \mathrm{d}\phi = 2 \left[(a+H)^3 - a^3 \right]. \tag{A2}$$

Re-arranging and dividing by a^3 yields

$$3\left(1 + \frac{H}{a}\right)^2 \int_{-\pi/2}^{\pi/2} \frac{\bar{\eta}(\phi)}{a} \cos\phi \, \mathrm{d}\phi + 3\left(1 + \frac{H}{a}\right) \int_{-\pi/2}^{\pi/2} \left(\frac{\bar{\eta}(\phi)}{a}\right)^2 \cos\phi \, \mathrm{d}\phi$$

$$+ \int_{-\pi/2}^{\pi/2} \left(\frac{\bar{\eta}(\phi)}{a}\right)^3 \cos\phi \, \mathrm{d}\phi = 0. \tag{A3}$$

To leading (first) order in $1/a$, we have

$$\int_{-\pi/2}^{\pi/2} \bar{\eta}(\phi) \cos\phi \, \mathrm{d}\phi \approx 0. \tag{A4}$$

Multiplying (4) by $\cos\phi$, integrating from $-\pi/2$ to $\pi/2$ and using the last expression yields (5), i.e.

$$\bar{\eta}\left(-\tfrac{1}{2}\pi\right) \approx \frac{a}{2g} \int_{-\pi/2}^{\pi/2} \mathrm{d}\phi \cos\phi \int_{-\pi/2}^{\phi} \left[2\Omega + \frac{\bar{u}}{a\cos\phi'} \right] \bar{u} \sin\phi' \, \mathrm{d}\phi'. \tag{A5}$$